A Smartphone-only Pulse Transit Time Monitor Based on Cardio-mechanical and Photoplethysmography Modalities

Chenxi Yang, Student Member, Yudi Dong, Student Member, Yingying Chen, Senior Member, Negar Tavassolian, Senior Member, IEEE

Abstract— This paper reports a system for monitoring pulse transit time (PTT). Using an Android smartphone and a customized sensing circuit, the system collects seismo-cardiogram (SCG), gyro-cardiogram (GCG), and photoplethysmogram (PPG) recordings. There is no need for any other external stand-alone systems. The SCG and GCG signals are recorded with the inertial sensors of the smartphone, while the PPG signal is recorded using a sensing circuit connected to the audio jack of the phone. The sensing circuit is battery-less, powered by the audio output of the smartphone using an energy harvester that converts audio tones into DC power. PPG waveforms are sampled via the microphone channel. A signal processing framework is developed and the system is experimentally verified on twenty healthy subjects at rest. The PTT is measured as the time difference between the aortic valve (AO) opening points in SCG or GCG and the fiducial points in PPG. The root-mean-square errors between the results from a stand-alone sensor system and the proposed system report 3.9 ms from SCG-based results and 3.4 ms from GCG-based results. The detection rates report more than 97.92% from both SCG and GCG results. This performance is comparable with stand-alone sensor nodes at a much lower cost.

Index Terms— gyro-cardiography (GCG), photoplethysmography (PPG), pulse transit time (PTT), seismocardiography (SCG), signal processing, smartphone, wearable sensors.

I. INTRODUCTION

CARDIOVASCULAR health is a significant public concern. According to the American Heart Association, approximately 11.5% of American adults have been diagnosed with some form of cardiovascular disease (CVD), and this number is expected to reach 45.1% by the year 2035 [1]. The economic cost of CVD is also expected to rise. In 2013, the annual cost of CVD in the United States was estimated as \$329.7 billion. This cost is expected to be increased to \$749 billion by 2035. Among all CVDs, hypertension has the highest occurrence among all demographic groups [1]. Providing an out-of-clinic, low-cost monitor can substantially increase the awareness ratio and reduce the associated costs of hypertension [2]. This will be hugely beneficial to a large population around the globe, especially in under-developed areas [3].

*Research supported by National Science Foundation (NSF) under award number 1855394.

Chenxi Yang and Yudi Dong are Ph.D. candidates at Stevens Institute of Technology, Hoboken, NJ, 07030 USA.

Yingying Chen is Professor of Electrical and Computer Engineering at Rutgers University, Piscataway, NJ, 08854 USA.

Negar Tavassolian is Associate Professor of Electrical Engineering at Stevens Institute of Technology, Hoboken, NJ 07030 USA. (e-mail: negar.tavassolian@stevens.edu).

Current non-invasive blood pressure (BP) monitoring methods are majorly cuff-based. However, most of these BP monitors cannot provide measurements in a continuous manner, i.e., they cannot effectively track immediate BP variations [4]. Immediate BP variations could potentially reveal the effectiveness of medication or treatment for hypertension. Medical doctors can cross-check the detected immediate BP variations and the activities of the subject to optimize the treatment [4], [5]. Automated alarm systems could also be developed by analyzing BP variations [6]. Moreover, they are inconvenient for long-term monitoring.

The arterial pulse transit time (PTT) is the time elapse of the blood pressure pulse when traveling from a proximal arterial site to a distal arterial location [4]. The velocity of this traveling pulse, named as the pulse wave velocity, is correlated with blood pressure [4], [7]. The variation of the pressure pulse can be recorded in a beat-to-beat manner. Therefore, PTT monitoring has been considered as a promising method for cuffless, continuous estimation of arterial BP [7].

Pulse arrival time (PAT) is commonly used as a surrogate of PTT in the literature [4]. PAT can be non-invasively measured as the traveling time of the pulse from the R-indices of the electrocardiogram (ECG) signal to the fiducial points of a photoplethysmogram (PPG) recording at a distal location [7]. However, the usefulness of employing PAT for BP monitoring has been interrogated as PAT contains the pre-ejection period (PEP), which might confound the results [4], [8].

Cardio-mechanical sensing, i.e., non-invasive sensing modalities that can be measured by inertial sensors, have been enthusiastically studied in recent years [9]-[11]. The seismocardiogram (SCG) is the vibrational signal recorded by placing accelerometers on the sternum of subjects, and the gyrocardiogram (GCG) is measured by placing gyroscopes at the same location as SCG measurements. Certain fiducial points on the SCG and GCG signals represent the aortic valve opening (AO) event [11], and can, therefore, provide proximal timing information for PTT estimation without the interference of PEP. In several recent works, a wearable sensor node has been used to record cardio-mechanical signals and PPG waveforms. They have shown that arterial PTT can be successfully extracted [12]-[14].

In most wearable monitoring literature, a stand-alone device collects the data and communicates with a smartphone or computer [12]-[15]. However, such a setup has several disadvantages. Firstly, the cost of a stand-alone device is high

as it is embedded with microprocessors and communication modules. Secondly, the battery life is generally restricted, limiting their capability for long-term monitoring. On the other hand, a smartphone-only solution could have a lower cost. The cost of the external hardware is lower, and there is no need for a stand-alone processor and communication module. The peripheral hardware will also have a better capability for longterm monitoring. The stand-alone device needs to stream the data continuously via wireless communication, which is powerconsuming. In comparison, the peripheral hardware can send data via cable with lower power consumption. On the other hand, there are tradeoffs when using a smartphone-only system. For instance, wearing a smartphone is less comfortable than wearing a small sensor node. The signal quality of the internal sensors of the smartphone might also be lower than that from a stand-alone system. It is to be noted that our goal is not to replace stand-alone designs by developing a smartphone-only solution. We are motivated to provide a low-cost alternative solution so that the financially-challenged population could also benefit from continuous and home-based monitoring of BP.

Smartphones have shown satisfactory performances in providing SCG and GCG signals using embedded inertial measurement units (IMU) [16]-[19]. In our preliminary works in [18] and [19], we investigated the feasibility of acquiring PTT signals with a smartphone for the first time. Specifically, the feasibility of extracting SCG and GCG waveforms from embedded IMUs were validated in [18]. However, the PPG signal was collected from a stand-alone device in [16] to evaluate the PTT accuracy. To evaluate a smartphone-only solution, a prototype circuit powered by the USB on-the-go (OTG) port of the smartphone was developed in [19]. A prototype PPG circuit built with off-the-shelf modules was implemented, and the PPG signal was sent via the audio jack of the phone. However, this prototype has several drawbacks. Firstly, the USB-OTG function is only supported in higher-end or newer models of smartphones [20], which influences the compatibility with a broader range of smartphone models. Furthermore, the signal acquisition circuit is power-consuming. Lastly, the signal quality is not satisfactory due to impedance and frequency matching challenges.

In this paper, we push our work forward by implementing a

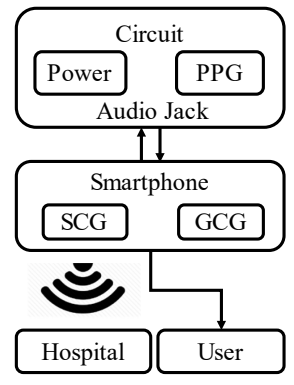


Fig. 1. The presented smartphone-only BP monitoring solution with the customized circuit powered and connected via the audio jack (modified from Fig.1 in [17]).

battery-less PPG circuit that harvests power from the audio output and sends the PPG signal through the microphone input of the smartphone. Most smartphone devices are equipped with an audio jack, which improves the compatibility of our system with various models of smartphones. A low-power sampling circuit is also developed that addresses the impedance and frequency matching challenges during the transmission of the PPG signal. Finally, the system is tested with an extended number of subjects.

Fig. 1 introduces the structure of the smartphone-only system in this work and the prospective application diagram. As illustrated in this figure, no external devices are needed. The smartphone can notify the user and when needed, communicate with care providers (e.g., clinics and hospitals) as a mobile communication device.

It is also worth mentioning that there are a few PPG-equipped smartphones which are capable of medical applications [15], [21], [22]. However, in these designs, the PPG sensor is embedded in the smartphone and needs to be firmly pressed to record the signal. This affects the mechanical coupling when the cell phone is placed on the chest wall. Therefore, the IMU will not be able to accurately record the cardio-mechanical signals and a simultaneous recording of cardio-mechanical and PPG signals will not be possible. Hence, an external PPG circuit is still necessary for smartphone-only PTT measurements.

The layout of the paper is as follows. In Section II, the methodology is introduced from hardware and software aspects. Section III summarizes the experimental setup and results, and Section IV provides discussions of the results. Section V introduces the conclusion and outlines future work.

II. METHODS

A. The Design of the Hardware System

The diagram of the hardware setup is illustrated in Fig. 2. In this setup, we compare the smartphone-only system with a stand-alone off-the-shelf reference device. The smartphone-only system consists of the smartphone hardware and the customized sensing circuit. The details are introduced in Section II.A.1 and Section II.A.2 respectively, followed by the reference device in Section II.A.3.

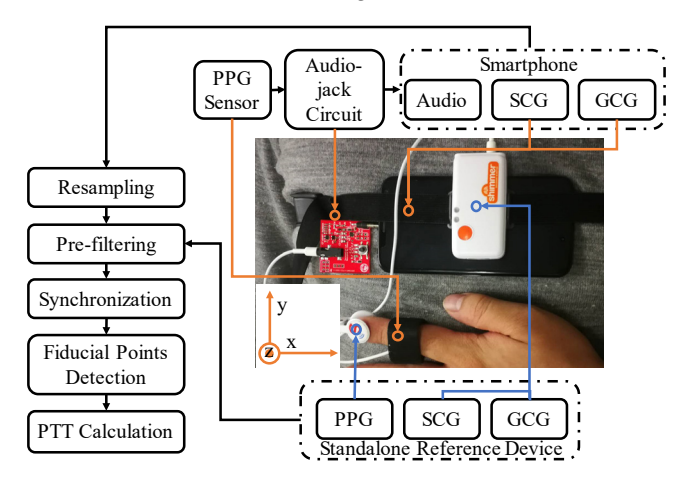


Fig. 2. The flowchart of the DSP infrastructure (left side) and a photo of the proposed hardware setup (right side).

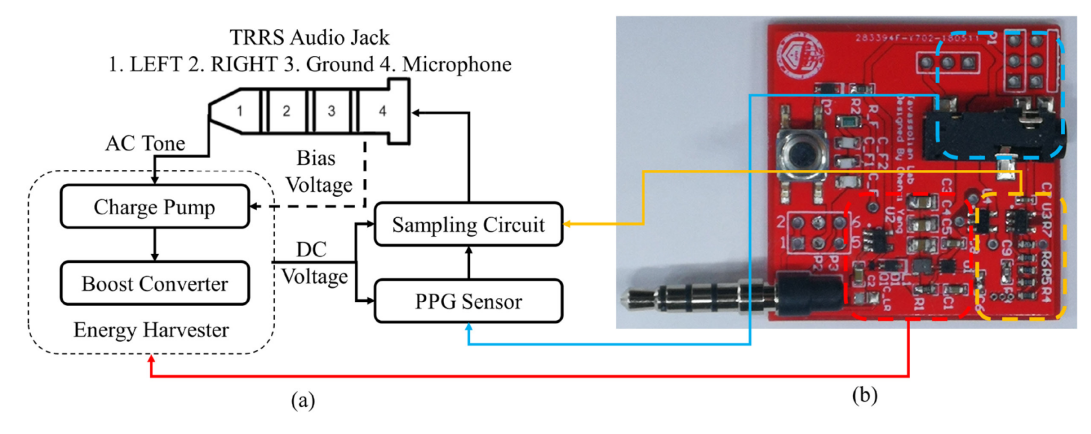


Fig. 3. (a) Block diagram of the hardware. (b) Design and physical layout of the PCB for the hardware.

1) Design of the Smartphone-only System

As illustrated in the right side of Fig. 2, a smartphone (Moto XT 1058) is attached to the subject based on the standard location of SCG/GCG sensing in [9], [11]. The smartphone is attached with a sport smartphone carrying strap, which is removed in Fig. 2 to show the overlay of the smartphone and the stand-alone sensor node device. The axis system is shown in Fig. 2. The backplate of the smartphone faces towards the chest wall so that the pitch and roll axes of the smartphone gyroscope match with the *x*- and *y*-axes respectively. In addition, the *z*-axis recordings of the smartphone accelerometer contain the vibration along the dorso-ventral axis of the subject. A customized PCB is connected to the audio jack, which handles the signal sampling of the PPG sensor located at the middle of the index finger. The detailed design of the PPG circuit for the smartphone is explained in the next sub-section.

2) The PPG Circuit Hardware Design

Fig. 3 (a) shows the diagram of the customized circuit. The circuit consists of three main parts: the audio jack interface, the energy harvester, and the PPG sampling circuit. The audio jack can output square or sine signals for AC power delivery via the audio channel. The energy harvester has a charge pump as the first stage, followed by a DC-DC boost converter. The charge

pump converts the AC output of one audio channel into an unregulated DC voltage, and the boost converter levels up the DC voltage to generate a regulated voltage of 3.3 V. The PPG sampling circuit and the PPG sensor are then powered by the DC voltage.

Firstly, a tip-ring-ring-sleeve (TRRS) 3.5-mm connector is used as the interface between the printed circuit board (PCB) and the smartphone. The pinout follows the CTIA standard [23]. As shown in Fig. 3, the tip (1) and the first ring (2) represent the left and right audio output channels from the smartphone. The second ring (3) represents the common ground. The sleeve (4) is the audio input to the smartphone, which is usually connected to a microphone. It is to be noted that in some smartphone models, the pin assignments of the ground and microphone are swapped [23]. We address this problem by implementing a hardware jumper cable to select pin allocations.

Secondly, an energy harvester is realized with the TPS610981 chip from Texas Instruments and a charge pump [24]. Fig. 4 shows the schematic of the energy harvester circuit. The charge pump receives the AC signal from the *Left* channel of the TRRS audio jack and converts it into an unregulated DC voltage. A bank of capacitors (C3-C5) hold the charge from the audio jack. An NMOS FET controlled by a low-power

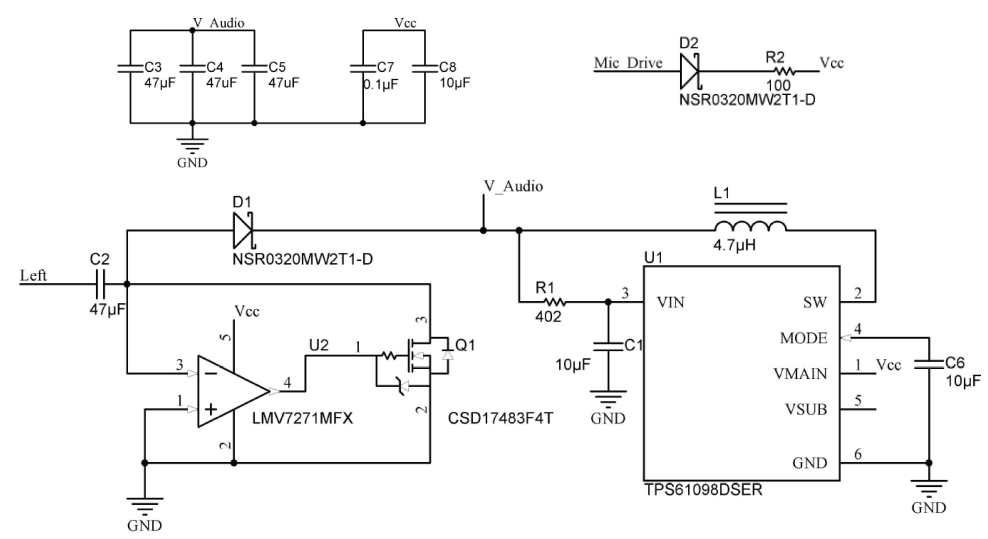


Fig. 4. Schematic of the energy harvester circuit (red square in Fig. 3 (b)).

comparator (LMV7271 from Texas Instruments), is implemented to mimic the function of a conventional diode. Before the input voltage of the boost converter rises, current will directly flow from the microphone input (Mic_Drive in Fig. 4) to V_{cc} through a Schottky diode (D2 in Fig. 4). V_{cc} will be charged to 1.8 V to start the comparator and the boost converter. The current path will be blocked when the converter enters regular operation, and V_{cc} outputs 3.3 V. The mode of the boost converter is set to low. The minimum startup voltage of the boost converter is 0.7 V. After the startup phase is finished, the input voltage can be as low as 0.4 V. The quiescent current of the boost converter is 300 nA under no-load condition, which is a suitable choice for such a low-power application.

Lastly, the PPG sensor (Shimmer sensing [25]) will be powered by the 3.3 V DC voltage. The maximum amplitude of the PPG signal is 2.8 V when powered with 3.3 V, which needs to be adjusted to match the input voltage of the audio jack of the smartphone. In addition, to ensure an effective signal transmission, the analog signal should be tuned to the audio range so that the ADC of the smartphone could adequately receive it. Therefore, we applied an analog switch (TS5A3166) controlled by a relaxation oscillator [26]. Fig. 5 presents the design of the relaxation oscillator with a comparator (LMV7271) and the analog switch. The RC values of the oscillator (R6 and C9 in Fig. 5 (a)) are tuned to generate a switching frequency of 1.424 kHz. The O out signal in Fig. 5 (a) controls the analog switch (U4 in Fig. 5 (b)). Therefore, the PPG signal is modulated, creating a composite signal within the audio passband. The signal that passes through the switch is then sampled and converted to proper impedance and voltage levels with a passive RC circuit. As shown in Fig. 5 (b), the signal from the PPG sensor is sent through a large resistor first

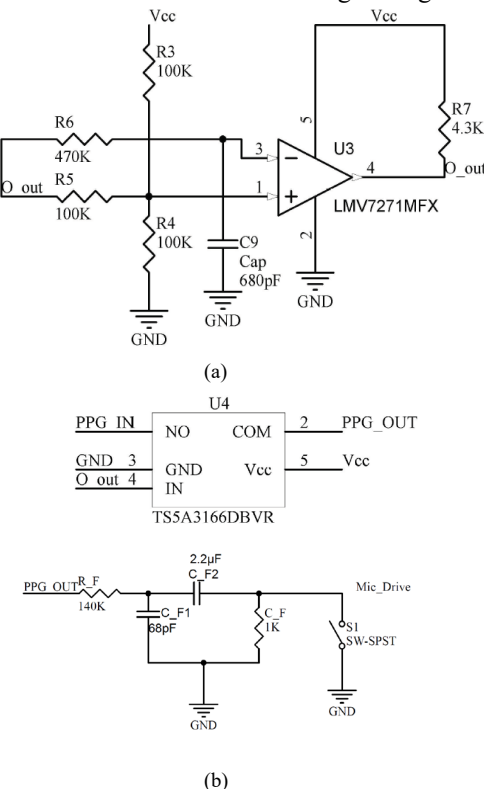


Fig. 5. (a) Structure of the relaxation oscillator and (b) structure of the analog switch and RC circuit.

 (R_F) . This resistor needs to be large enough for converting the voltage level. In this case, it is 140 K Ω . Another 1-K Ω resistor is connected to ground so that the smartphone can detect the circuit as a microphone. C_F2 is included to isolate the DC bias and C_F1 is used to reject high-frequency noise [23].

In addition to the three main parts, a button is added as a trigger for the synchronization as shown in Fig. 5 (b). The button is connected to the microphone channel with a standard impedance of 0 Ohm to ground to mimic the behavior of Function A in the Android development standard [23].

3) The Stand-alone System Setup

A wearable sensor node (Shimmer 3 from Shimmer Sensing [25], pointed by the blue arrow in Fig. 2) is placed on top of the smartphone with an elastic strap. The capability of measuring valid PTT values with the Shimmer sensor node setup has been verified in [12].

The SCG signal is measured by a three-axis accelerometer, and a three-axis gyroscope records the GCG. Moreover, a PPG sensor is connected to the tip of the same finger used in the smartphone-only setup. It is to be noted that although the attachment methods of the two PPG sensors are different, their characteristics and performances are identical as the same model of the optical sensing circuit is used in both designs [25]. This ensures a fair comparison of the PPG waveforms. The accelerometer is limited to ± 2 g, while the gyroscope is limited to ± 250 degrees-per-second (DPS). The sampling rate is 256 Hz for all the sensors.

B. The Software System

Besides the hardware system, a smartphone application and a DSP framework are developed based on the software developed in [19]. The smartphone application is introduced in Section II.B.1, followed by the DSP program.

1) Design of the Smartphone Application

There are three major activities in this Android program, which handles three main tasks. The first task is the datalogging of SCG and GCG signals based on the *SensorEvent* with *SensorEventListener*. The nominal sampling frequency used in the study is set to 180 Hz [19]. We extract the *gyro_roll* data as the GCG signal which corresponds to the *y*-axis. The *acceleration data* from *z-axis* is used as the SCG signal.

Secondly, an audio-recording activity based on the standard Android *MediaRecorder* is applied to record the PPG signal. The configuration of this activity is introduced in [19]. Based on the method used in [12], we compensate for the delay of the audio recordings due to the audio front-end of the smartphone. The sampling frequency of the audio ADC is 44,100 Hz for the smartphone used in this work. This value might be different in other models of smartphones.

Finally, a third activity plays a tone of a 5-kHz sine wave and generates the output via the left audio output. The button trigger in *Function* A calls the management of the synchronization between the three activities [23].

2) Structure of the DSP Framework

Fig. 2 shows the framework of the digital signal processing

TABLE 1 A VERAGE 1 1 I MEASUREMENT RESULTS IN MILLI-SECONDS													
Subject	PTT from smartphone		PTT from reference device			PTT ₂ -	r.Ī/	PTT from smartphone		PTT from reference device		PTT ₁ - PTT ₃ /	PTT ₂ - PTT ₄ /
						PTT_4 /							
	PTT ₁	PTT,	PTT ₃	PTT ₄	PTT ₃	PTT ₄	Subject	PTT ₁	PTT ₂	PTT ₃	PTT ₄	PTT ₃	PTT ₄
	(SCG)	(GCG)	(SCG)	(GCG)	(%)	(%)		(SCG)	(GCG)	(SCG)	(GCG)	(%)	(%)
1	164.2	163.9	167.6	166.7	2.03%	1.68%	11	208.8	198.2	204.1	202.7	2.30%	2.22%
2	178.5	178.2	174.2	174.1	2.47%	2.35%	12	163.5	160.7	164.8	165.1	0.79%	2.67%
3	148.3	153.7	153.9	151.8	3.64%	1.25%	13	179.2	181.8	177.6	177.4	0.90%	2.48%
4	177.1	177.1	179.2	178.3	1.17%	0.67%	14	137.1	142.5	140.2	141.1	2.21%	0.99%
5	169.2	165.3	163.7	162.8	3.36%	1.54%	15	201.2	206.3	207.3	207.8	2.94%	0.72%
6	168.4	169.4	165.3	166	1.88%	2.05%	16	181.7	188.9	183.5	182.5	0.98%	3.51%
7	164.3	169.6	168.1	167.2	2.26%	1.44%	17	178.6	180.1	182.2	182.7	1.98%	1.42%
8	161.2	151.8	155.2	155.7	3.87%	2.50%	18	168.8	169.2	166.3	167.4	1.50%	1.08%
9	180.1	186.1	185.4	184.7	2.86%	0.76%	19	177.5	175.4	173.9	172.5	2.07%	1.68%
10	194.7	197.5	193.2	194.6	0.78%	1.49%	20	157.7	160.3	154.8	155.2	1.87%	3.29%

TABLE I AVERAGE PTT MEASUREMENT RESULTS IN MILLI-SECONDS

program. Single-axis SCG from the z-axis is used from the smartphone system and the reference system [9]. The GCG signals are selected from the *y*-axis of the stand-alone sensor and the gyro_*roll* axis of the smartphone. The GCG from *y*-axis is reported to have a high signal quality [10], [11].

The recordings from the smartphone are resampled to 128 Hz. The PPG recordings are uniformly resampled while the SCG and GCG recordings are non-uniformly resampled via a spline interpolation to improve the signal quality. More details of the resampling could be found in [18].

All signals are then pre-filtered with a zero-phase infinite impulse response (IIR) bandpass filter. The seismo-cardiogram (SCG) and gyro-cardiogram (GCG) signals are filtered from 0.8 Hz to 25 Hz to focus on the infrasonic band. The PPG signals are filtered from 0.8 Hz to 60 Hz. Afterwards, all the recordings are synchronized. The synchronization between smartphone IMU and PPG recordings is based on the compensation of the timestamp differences, while the synchronization between devices is based on a tapping method as explained in detail in [19]. Following the synchronization step is the fiducial points extraction. The systolic maximum point is referred as the distal time indicator from PPG [11]. The indices of the PPG distal points are denoted as $T_{PPG}(i)$. The proximal pulse time in SCG and GCG are then located with the following equations.

$$IM_{SCG}(i) = \operatorname{minimum}_{t=T_{PPG}(i)}^{T_{PPG}(i+1)}(SCG)$$
 (1)

$$AO_{SCG}(i) = \text{maximum}_{t=IMSCG(i)}^{IM(i)+200ms}(SCG)$$
 (2)

$$AO_{GCG}(i) = \text{maximum}_{t=T_{PPG}(i)}^{T_{PPG}(i+1)}(GCG)$$
 (3)

In these equations, *i* represents the peak indices. The maximum and minimum are functions that find the indices of the maximum or minimum values in a certain range. In (1), *IM*(*i*) is the index of the minimum point between two consecutive PPG peaks. This fiducial point biophysically represents the isovolumic moment (IM) of the heart activity. Then the indices of the first maxima within the time range of 200 ms after each IM point in the SCG signal are located. These peaks are referred to as the aortic valve opening (AO) points, which is shown in (2). (3) explains the detection of AO from GCG which is explained in detail in [9].

Four different PTT values, defined as PTT_{1-4} , are then calculated. PTT_{1-2} are calculated from AO_{SCG} to T_{PPG} and AO_{GCG} to T_{PPG} respectively from smartphone recordings. PTT_{3-4} are the same calculations based on the stand-alone device from AO_{SCG} and AO_{GCG} to the T_{PPG} , successively. Consistent with our previous study [19], a valid PTT is defined as a measurement in which the error range is within 50% of the reference value. An invalid PTT is considered as a failure in detection, which will be used for evaluating the detection rate of PTT cycles. In addition to this comparison, we also consider the standard error range of 10% according to the American National Standards [28].

III. EXPERIMENTAL SETUP AND RESULTS

A. Experimental Setup and Protocol

First, characterization experiments were conducted in a climate-controlled lab environment. The power consumption of each component was measured by manually disabling the surrounding circuits and measuring the voltage and current values.

Human experiments were conducted on twenty healthy adult subjects. The experimental protocol was approved by the Committee for the Protection of Human Subjects at Stevens Institute of Technology (protocol number 2017-008AR1). The subjects were asked to stay in a supine position on a bed for 5 minutes. The subjects were asked to breathe naturally. The average age, height, and weight are 24.6 years old, 67.4 inches and 138.2 lbs.

B. Experimental Results

1) Power Consumption Results

The power consumption is measured with a multimeter (HP 34401A, Keysight Technologies). Both the standby and working currents are measured as an average of current in 5 minutes. The standby current is 88 μ A when the output voltage is 3.28 V, which translates to 289 μ W of power consumption. The peak working power reports 3.426 mW (1.04 mA @ 3.29 V). The breakdown of power consumption is shown in Fig. 6. It is seen that the sampling circuit takes 47% of the power with

1.608 mW. The PPG sensor consumes 1.527 mW (0.46 mA @ 3.29 V), which represents 45% of the power. The energy harvester and other components of the circuit occupy 8% of the power consumption. It is seen that the sampling circuit consumes the most significant portion of the total power. The PPG circuit consumes slightly less power, i.e., 45% as compared to 47% from the sampling circuit. This distribution suggests that disabling both the sampling circuit and the PPG sensor are critical if a low standby power consumption is desired.

In comparison, the previous prototype in [19] takes more than 10 mW from the USB-OTG port with the same PPG sensor. This result indicates that the proposed design is significantly improved in power consumption, which could lead to a longer monitoring capability.

Compared to other PPG systems, the benchtop system of PPG100C with TSD 124 from BIOPAC consumes 30 mW [29]. The PPG circuit from a state-of-the-art wristband wearable sensor consumes 172 μ W and the whole system consumes 1.66 mW [30]. The PPG ASIC in another study consumes 2.6 μ W [31]. Our results are better than benchtop systems but much lower than the state-of-the-art PPG circuits.

2) PTT Estimation Errors

Table I shows the PTT error results from all subjects. PTT_1 and PTT_3 are based on SCG fiducial points from smartphone and stand-alone reference devices, respectively. PTT_2 and PTT_4 are based on GCG fiducial points.

From the PTT measurements based on SCG, the maximum percentage error between PTT_1 and PTT_3 is 3.87% (subject 8). The average percentage error from the SCG-based method is 2.09%, with an RMSE of 3.9 ms.

On the other hand, the largest percentage error between GCG-based PTT_2 and PTT_4 is 3.51% (Subject 16). On average, the percentage error between PTT_2 and PTT_4 is 1.79%. The RMSE reports 3.4 ms.

Statistical results suggest that the GCG-based method outperforms the SCG-based method in both the average percentage error (1.79% vs. 2.09%) and RMSE (3.4 ms vs. 3.9 ms). Furthermore, the correlation coefficient between SCG- and GCG-based values reports 0.994 (p < 0.005), which suggests high agreement between the two results.

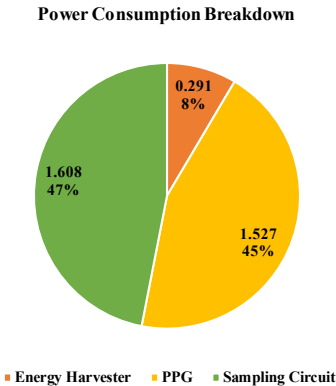


Fig. 6. Power consumption breakdown of the PPG circuit.

In conclusion, GCG-based PTT results outperform SCG-based results, which is consistent with our previous work [19]. The Bland-Altman plot between PTT_2 and PTT_4 is shown in Fig. 7. The PTT values are based on GCG waveforms from one representative measurement. It indicates that the PTT results from the smartphone track the corresponding results from the reference sensor with a high agreement level.

3) PTT Detection Rates

In summary, 2697 PTT cycles are collected from 20 subjects. The detection rate is calculated by dividing the number of valid PTT cycles defined in Section II.B.2 by the total number of PTT cycles [19]. Based on the 50% standard, the detection rates of PTT from all subjects are 97.92% (2641/2697) from SCG and 98.55% (2658/2697) from GCG. Based on the 10% standard, the detection rates of PTT are 95.96% (2588/2697) from SCG and 96.89% (2613/2697) from GCG. It is seen that the results from GCG are slightly superior to the results from SCG.

IV. DISCUSSION

A. Comparison between the Proposed Work and Previous Results

Table II summarizes the statistical results from this work and other designs. The first three rows show the comparison between this work and the work in [19]. It is observed that both the RMSE and absolute error are smaller in this work compared to the results from [19]. The RMSE from SCG is improved from 4.77 ms to 3.89 ms. Furthermore, the RMSE from GCG drops from 3.93 ms to 3.37 ms. Particularly, the RMSE from SCG in this work is now comparable with the RMSE of GCG from the previous work. Similar observations could also be found in the absolute error trends. The results suggest that the accuracy of PTT extraction has been improved due to the improved quality of the PPG signal.

Also, the detection rate of a valid PTT has been increased significantly from 92.75% to 97.92% based on SCG results and from 93.63% to 98.55% based on GCG results. The improvement in detection rates reveals the benefit of increased PPG signal quality and robustness.

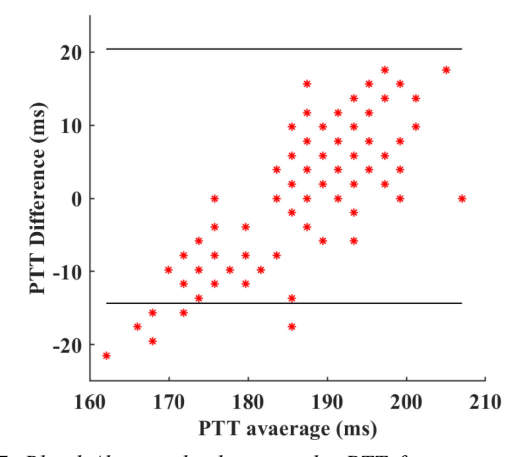


Fig. 7. Bland-Altman plot between the PTT from smartphone-only system and the PTT from the stand-alone device. The recordings are from one representative recording of GCG waveforms (black horizontal lines represent the 95% agreement limit borders).

Table II Comparison Between the This Work and the Previous Work

(ERROR VALUES ARE IN AVERAGE IN MILLI-SECONDS)

	RM	1SE		olute ror	Detection Rate		
	SCG	GCG	SCG	GCG	SCG	GCG	
This work	3.89	3.37	3.59	3.07	97.92%	98.55%	
Results in [19]	4.77	3.93	4.01	3.24	92.75%	93.63%	

B. Comparison with Other Self-Powered Designs

There are several other designs in the literature that focus on harvesting energy from the audio jack of smartphones for sensor circuits [32]-[35]. The specs from these papers are summarized in Table III. In [32], the AC signal from one audio channel was converted with a transformer to power a microprocessor. The microphone channel was used as a digital channel to send data back to the smartphone. The energy harvester delivers 7.4 mW of power with an operating voltage of 2.8 V. In [33], the microphone bias voltage was used as the power source. The energy harvester is based on linear voltage regulars and provides energy for an electrocardiogram (ECG) circuit, which consumes 216 µW at 1.8 V. The maximum power delivery is 322 µW via an iPhone. In [34] and [35], both the left and right audio channels were used to generate frequency shift keying (FSK) modulation signals. A transformer design similar to [32] was implemented in [34] to convert the FSK signal to DC power, which delivers a maximum power of 31.7 mW at 1.8V. In [35], an array of Schottky diodes was used to convert the FSK waveforms, which can provide 36.3 mW of power at 1.91 V. A microprocessor is included in the design of both [32] and [34]. It is seen that the designs with digital communications implement transformers and diode arrays for higher power capacity [32], [34], [35]. They can deliver more power than the solution that relies on the bias circuit [33].

In this work, the peak power of our design is 3.426 mW at 3.3 V. We need higher power capability than the bias-only design in [33], but less power than the designs which implement digital communications and microprocessors. Therefore, the audio signal is selected as the main power source via a charge pump while the bias voltage is used as the step-up supportive voltage source. Since there is no need for transformers or an array of diodes, the form factor of our design has a better miniaturization potential. For example, the effective energy harvester size in [32] is about 225 mm². In comparison, the effective circuit size in our design is approximately 200 mm². Our solution achieves a balance between form factor and power capability, which is suitable for applications that require higher than μW power levels as well as direct analog readings.

C. Cost Breakdown and Comparison

Table IV summarizes the cost of the major parts of the hardware circuit. The design uses analog chips and passive components that are active in production. As a result, the estimated cost is \$4.38. Similar to the cost breakdown in [33], this cost analysis includes everything except for the PPG sensor. In comparison, the designs in [33] cost \$5 for 10 k units

TABLE III COMPARISON BETWEEN THE PRESENTED WORK AND OTHER DESIGNS

	Self-powered Design Comparison					
	Power	Voltage	Method			
This work	3.426 mW	3.3 V				
[32]	7.4 mW	2.8 V	Transformer			
[33]	216 μW	1.8 V	Mic Bias			
[34]	31.7 mW	1.8 V	Transformer			
[35]	36.3 mW	1.91 V	Diode Array			

(sensor excluded), slightly higher than the cost of our system.

Considering the average price of a typical PPG sensor at about \$5 [36], the total price of our hardware will be less than \$10. This suggests a very low-cost solution.

V. CONCLUSIONS

This paper presents a novel PTT monitoring solution using the embedded sensors of a smartphone and a customized circuit. The smartphone-only design shows comparable performance to a commercial stand-alone device [11]. Both the detection accuracy and detection stability are higher than the results of previous studies [19]. The power consumption of the circuit is also reduced due to the low-power design.

One limitation of the proposed design is that the power delivery is not dynamic based on the load change. In future studies, we will investigate a feedback-controlled power delivery by changing the frequency and amplitude of the toned sine wave which is sent to the energy harvester [37]. Additionally, power distribution results indicate that the PPG sensor and the sampling circuit should be disabled to achieve a low standby power. In the future, a power management circuit will be implemented to control the active load configurations. Furthermore, the quality of SCG and GCG waveforms could potentially be improved using multi-axis sensor fusion [38]. The sampling rate of the smartphone IMU also limits the performance of the system. Wearing a smartphone is less comfortable than wearing a small sensor node, which might result in some tradeoffs in convenience. Other fiducial points from the PPG waveform could be used for PTT calculation to improve the stability of the system under more application scenarios. Finally, alternative PPG locations that can provide a more comfortable setup such as the earlobe will be evaluated.

Our future work also includes the evaluation of the system

Table IV Cost Breakdown of The Hardware (values are based on $10 \, \mathrm{k}$ units)

Part	Manufacturer	Model	Cost
Charge Pump	TI	LM7271	0.47
Boost Converter	TI	TPS61082	0.66
Sampling Comparator	TI	LM7271	0.47
Analog Switch	TI	TS5A3166	0.16
TRRS connector	Tensility	54-00035	1.77
PCB	NOA Labs	N/A	0.40
Passives	N/A	N/A	0.45
Total	_	_	4.38

capability in providing beat-to-beat BP estimates. Continuous monitoring of blood pressure could improve the detection and management of hypertension by showing real-time analysis to the users [4], [22]. This work shows promising potential in monitoring PTT and BP at home or in low-resource areas with a low cost.

REFERENCES

- [1] E. Benjamin, et al. "Heart disease and stroke statistics-2018 update: a report from the American Heart Association." Circulation, vol. 137, no.12, 2018.
- Y. L. Zheng, et al., "Unobtrusive Sensing and Wearable Devices for Health Informatics," *IEEE Tran. on Biomed. Eng.*, vol. 61, no. 5, pp. 1538-1554, May 2014.
- J. Andreu-Perez, et al., "From Wearable Sensors to Smart Implants-Toward Pervasive and Personalized Healthcare," IEEE Tran. on Biomed. Eng., vol. 62, no. 12, pp. 2750-2762, Dec. 2015.
- [4] R. Mukkamala, et al., "Toward Ubiquitous Blood Pressure Monitoring via Pulse Transit Time: Theory and Practice," *IEEE Trans. on Biomed. Eng.*, vol. 62, no. 8, pp. 1879-1901, Aug. 2015.
- P. Fung, et al., "Continuous Noninvasive Blood Pressure Measurement by Pulse Transit Time," The 26th annual international conference of the *IEEE engineering in medicine and biology society*, pp. 738-741, 2004.
- Y. Yoon, et al., "Non-Constrained Blood Pressure Monitoring Using ECG and PPG for Personal Healthcare," Journal of Medical Systems, vol. 33, no. 4, pp. 261-266, 2009. H. Gesche, *et al.*, "Continuous Blood Pressure Measurement by Using the
- Pulse Transit Time: Comparison to a Cuff-Based Method," Eur. J. Appl. Physiol., vol. 112, pp. 309–315, 2012.
 G. Zhang, et al., "Pulse Arrival Time is not an Adequate Surrogate for
- Pulse Transit Time as a Marker of Blood Pressure," J. Appl. Physiol., vol. 111, pp. 1681–1686, 2011.
- Paukkunen, Mikko. "Seismocardiography: Practical Implementation And Feasibility." PhD Dissertation, Dep. of Elec. Eng. and Auto., Aalto University, 2014.
- [10] Tadi Mojtaba Jafari, et al., "Gyrocardiography: A New Non-invasive Monitoring Method for the Assessment of Cardiac Mechanics and the Estimation of Hemodynamic Variables." Sci. Reports, vol.7, 2017.
- C. Yang, N. Tavassolian, "Combined Seismo- and Gyro-cardiography: A More Comprehensive Evaluation of Heart-Induced Chest Vibrations," IEEE J. of Biomed. and Health Info., vol. 22, no. 5, pp. 1466-1475, Sept.
- [12] C. Yang and N. Tavassolian, "Pulse Transit Time Measurement Using Seismocardiogram, Photoplethysmogram, and Acoustic Recordings: Evaluation and Comparison," in IEEE J. of Biomed. and Health Info., vol. 22, no. 3, pp. 733-740, May 2018.
 [13] M. Di Rienzo, et al., "A new technological platform for the multisite
- assessment of 3D seismocardiogram and pulse transit time in cardiac patients," 2016 Computing in Cardio. Conf. (CinC), Vancouver, BC, 2016, pp. 781-784.
 [14] A. K. Verma, *et al.* "Pulse Transit Time Derivation using Xiphoidal and
- Carotid Seismocardiograms." 2017 Design of Med. Devices Conf. American Soc. of Mech. Engineers, pp. V001T01A010-V001T01A010,
- [15] Anand Chandrasekhar, et al, "Smartphone-Based Blood Pressure Monitoring via The Oscillometric Finger-Pressing Method." Science translational medicine, vol. 10, no. 431, 2018.
- O. Lahdenoja, et al., "A Smartphone-Only Solution For Detecting Indications Of Acute Myocardial Infarction," 2017 IEEE Int. Conf. on Biomed. & Health Info. (BHI), Orlando, FL, 2017, pp. 197-200.

 [17] O. Lahdenoja, et al., "Atrial Fibrillation Detection via Accelerometer and
- Gyroscope of a Smartphone," in IEEE J. of Biomed. and Health Info., vol.PP, no.99, pp.1-1, 2017.
- [18] C. Yang, N. Tavassolian, "A feasibility study on a low-cost, smartphonebased solution of pulse transit time measurement using cardio-mechanical signals," 2017 IEEE Health. Inno. and Point of Care Tech. (HI-POCT),
- pp. 93-96. C. Yang, Y. Dong, Y. Chen and N. Tavassolian, "A Low-cost, Smartphone-only Pulse Transit Time Measurement System Using Cardio-mechanical Signals and Optical Sensors," 2018 40th Annual International Conference of the IEEE Engineering in Medicine and Biology Society (EMBC), Honolulu, HI, 2018, pp. 1-4.doi: 10.1109/EMBC.2018.8513270
- [20] Prashant S. Mulay, et al. "Power Harvesting Through Headphone Jack of Android Smartphone for Low Power Medical Devices." International Conference on Intelligent Computing and Control Systems (ICICCS). IEEE, 2017.
- [21] A. Gaurav, et al., "Cuff-Less PPG Based Continuous Blood Pressure Monitoring — A Smartphone Based Approach," 2016 38th Annual

- International Conference of the IEEE Engineering in Medicine and
- Biology Society (EMBC), Orlando, FL, 2016, pp. 607-610.
 [22] Kenta Matsumura, et al. "Cuffless Blood Pressure Estimation Using Only
- A Smartphone." *Scientific reports*, vol. 8, no. 1, pp.7298, 2018.

 [23] "3.5 mm Headset: Accessory Specification" [Online] Availble at: https://source.android.com/devices/accessories/headset/plug-headset-
- "PMP9777" [Online] Available at: http://www.ti.com/tool/PMP9777
 "Shimmer Sensing PPG to HR" [Online] Available at: http://ww v.shimmersensing.com/products/ppg-to-hr-ear-cilp#related-tab
- [26] Clayton, George Burbridge, and Steve Winder. Operational amplifiers. Elsevier, 2003.
- [27] "Shimmer 3" [Online] Available at: http://www.shimmersensing.com/ products/shimmer3-wireless-gsr-sensor
- [28] Cardiac monitors, heart rate meters, and alarms. Arlington: American National Standards Institute, Inc.; 2002
- https://www.biopac.com/product/spo2-transducers
- P. Ahmmed, et al., "A Wearable Wrist-Band with Compressive Sensing based Ultra-Low Power Photoplethysmography Readout Circuit," IEEE 16th International Conference on Wearable and Implantable Body Sensor Networks (BSN), 2019.
- [31] A. Caizzone, A. Boukhayma, and C. Enz, "A 2.6µW Monolithic CMOS Photoplethysmographic Sensor Operating with 2µW LED Power," 2019 IEEE International Solid- State Circuits Conference - (ISSCC), San Francisco, CA, USA, 2019, pp. 290-291.
- [32] Y.S. Kuo, et al., "Hijacking power and bandwidth from the mobile phone's audio interface." Proceedings of the First ACM Symposium on Computing for Development, pp. 24, 2010.
- Sonal Verma, Andrew Robinson, and Prabal Dutta. "AudioDAQ: Turning the Mobile Phone's Ubiquitous Headset Porti into A Universal Data Acquisition Interface." In Proceedings of the 10th ACM Conference on Embedded Network Sensor Systems, pp. 197-210. ACM, 2012
- [34] Z. Li and H. Nie, "Implementation of A Joint Power Harvesting and Communication Technology on A Smartphone's 3.5 mm Audio Interface," 2018 IEEE International Conference on Electro/Information Technology (EIT), Rochester, MI, 2018, pp. 0747-0752.
 [35] H. Nie, R. Joshi and Z. Li, "An improved joint power harvesting and
- communication technology for smartphone centric ubiquitous sensing applications," 2016 13th IEEE Annual Consumer Communications & Networking Conference (CCNC), Las Vegas, NV, 2016, pp. 44-48.
- "High-Sensitivity Pulse Oximeter and Heart-Rate Sensor for Wearable Health" [Online] Available at: https://www.maximintegrated.com/en/ products/sensors/MAX30102.html/
- Alexander C. Sun, et al., "An Efficient Power Harvesting Mobile Phone-Based Electrochemical Biosensor for Point-Of-Care Health Monitoring.' Sensors and Actuators B: Chemical, vol. 235, pp. 126-135, 2016.
- [38] H. Lee, H. Lee, M. Whang, "An Enhanced Method to Estimate Heart Rate from Seismocardiography via Ensemble Averaging of Body Movements At Six Degrees Of Freedom." Sensors, vol. 18, no. 1, pp.238, 2018.



Chenxi Yang (S'13) received the B. Eng. degree in Measuring Control Technology & Instruments from Southeast University, Nanjing, China, in 2013, and the M. Eng. degree in electrical engineering from Stevens Institute of Technology, Hoboken, NJ, in 2015. He is currently working towards his Ph.D. in electrical engineering at Stevens

Institute of Technology. His research interests are biophysical signal processing and mobile healthcare with sensor networks. He is a student member of the IEEE Signal Processing Society, Circuits and Systems Society, and Engineering in Medicine and Biology Society. He has received the Edward Peskin Award for an Outstanding Master's Thesis at Stevens Institute, a conference travel award for his paper at BIOCAS 2015, Atlanta, GA, and the NSF EMBC Award for Young Professionals on Smart and Connected Health at EMBC 2016, Orlando, FL.



Yudi Dong (S'17) received the B.Eng. degree in optoelectronic information engineering from University of Shanghai for Science and Technology, Shanghai, China, in 2014, and the M.Sc. degree in electrical engineering from Stevens Institute of Technology, Hoboken, NJ,

USA, in 2017, where he is currently pursuing the Ph.D. degree. His current research interests include deep learning and mobile security.



Yingying (Jennifer) Chen is a Professor of Electrical and Computer Engineering at Rutgers University and the Associate Director of Wireless Information Network Laboratory (WINLAB). She also leads the Data Analysis and Information Security (DAISY) Lab. Her research interests

include smart healthcare, cyber security and privacy, Internet of Things, and mobile computing and sensing. She has co-authored three books, published over 150 journals and referred conference papers and obtained 8 patents. Her background is a combination of Computer Science, Computer Engineering and Physics. Prior to joining Rutgers, she was a tenured professor at Stevens Institute of Technology and had extensive industry experiences at Nokia (previously Alcatel-Lucent). She is the recipient of the NSF CAREER Award and Google Faculty Research Award. She also received NJ Inventors Hall of Fame

Innovator Award. She is the recipient of multiple Best Paper Awards from IEEE CNS 2018, IEEE SECON 2017, ACM AsiaCCS 2016, IEEE CNS 2014 and ACM MobiCom 2011.



Negar Tavassolian (S'03–M'11–SM'18) is an Associate Professor at the Department of Electrical and Computer Engineering at Stevens Institute of Technology, where she directs the Bio-Electromagnetics Laboratory. She received the B.Sc. and M.Sc. degrees in electrical engineering from Sharif University of Technology,

Tehran, Iran, and McGill University, Montreal, Canada, in 2003 and 2006, respectively. She received the Ph.D. degree in electrical engineering from Georgia Institute of Technology in 2011 and was a Postdoctoral Associate at the David H. Koch Institute for Integrative Cancer Research at Massachusetts Institute of Technology from 2011 to 2013. Dr. Tavassolian was an Assistant Professor at Stevens Institute of Technology from 2013 to 2019. She is a recipient of the NSF CAREER award in 2016 and the Provost Early Career Award for Research Excellence in 2018. She is a senior member of IEEE since 2018 and a Technical Program Committee member of IEEE MTT-10: Biological Effects and Medical Applications of RF and Microwaves since 2015. Her research is funded by the National Science Foundation and the US Army Medical Research and Material Command.